Palo, M., Tilmann, F., Schurr, B. (2016): Applicability and Bias of VP/VS Estimates by P and S Differential Arrival Times of Spatially Clustered Earthquakes V S Estimates by P and S Differential Arrival Times of Spatially Clustered Earthquakes. - *Bulletin of the Seismological Society of America*, *106*, 3, pp. 1055—1063.

DOI: http://doi.org/10.1785/0120150300

THE SEISMOLOGICAL SOCIETY OF AMERICA
400 Evelyn Ave., Suite 201
Albany, CA 94706-1375
(510) 525-5474; FAX (510) 525-7204
www.seismosoc.org

Bulletin of the Seismological Society of America, Vol. 106, No. 3, pp. 1055–1063, June 2016, doi: 10.1785/0120150300

Applicability and Bias of V_P/V_S Estimates by P and S Differential Arrival Times of Spatially Clustered Earthquakes

by Mauro Palo, Frederik Tilmann,* and Bernd Schurr

Abstract Estimating small-scale V_P/V_S variations at depth can be a powerful tool to infer lithology and hydration of a rock, with possible implications for frictional behavior. In principle, from the differential arrival times of P and S phases from a set of spatially clustered earthquakes, an estimate of the local V_P/V_S can be extracted, because the V_P/V_S is the scaling factor between the P and S differential times for each pair of earthquakes. We critically review the technique proposed by Lin and Shearer (2007), in which the mean value over all stations is subtracted from the differential arrival times of each pair of events in order to make the method independent of *a priori* information on origin times. The demeaned differential P and S arrival times are plotted on a plane, and the V_P/V_S ratio is estimated by fitting the points on this plane.

We tested the method by both theoretical analysis and numerical simulations of P and S travel times in several velocity models. We found that the method returns exact values of V_P/V_S only in the case of a medium with homogeneous V_P/V_S, whereas, when a V_P/V_S gradient is present, the estimates are biased as an effect of systematic differences between P and S takeoff angles. We demonstrated that this bias arises from the demeaning of the arrival times over the stations. In layered models with V_P/V_S decreasing with depth, we found that V_P/V_S is overestimated or underestimated, respectively, for takeoff angles larger or smaller than 90°. Moreover, we calculated analytically the dependence of this bias on the takeoff angles.

Our simulations also showed that the difference between the calculated and the expected V_P/V_S is reduced for simple horizontally layered velocity structures (<0.06), whereas it is 0.27 in a more realistic velocity model mimicking a subduction zone.

Introduction

The ratio between the seismic velocities of P and S waves ($\gamma = V_P/V_S$ hereafter) is a useful physical parameter to define the lithological properties of crustal and mantle rocks (e.g., O'Connell and Budiansky, 1974; Christensen, 1996; Hacker *et al.*, 2003; Wang *et al.*, 2012). This parameter is also very sensitive to the presence of fluids, which at crustal depths are often present in the form of high-pressure water-filling pores and fractures in the rock (e.g., Lachenbruch, 1980; Shearer, 1988; Audet *et al.*, 2009; Peacock *et al.*, 2011). Fluids can also affect the frictional properties of faults, thus determining different regimes of failure (strike-slip, stable-creeping, and slow-slip events) (e.g., Lay and Kanamori, 1981; Scholz, 1998; Schwartz and Rokosky, 2007).

On a small scale, estimates of γ are usually inferred by mechanical experiments on rock samples (e.g., Eberhart-Phillips *et al.*, 1989) or from drill logs (e.g., Hickman and Ellsworth, 2010). Under certain conditions, it was proposed that γ can be estimated *in situ* from the differential P and S travel or arrival times of pairs of events of a spatially clustered set of earthquakes (Lin and Shearer, 2009; Dahm and Fischer, 2014). Here we test the method proposed by Lin and Shearer (2007) with a set of synthetic cases, extending the scenarios examined in the original paper and thus further describing the limitations and the range of applicability of the technique.

Method

Theoretical Background

Lin and Shearer (2007) proposed a method that returns an estimate of γ in the area of a spatially clustered set of earthquakes. In this method, it is assumed that (a) the events of the cluster are close together enough that the seismic velocity is locally constant; (b) the P and S reciprocal wave-

*Also at Freie Universität, Fachrichtung Geophysik, Berlin, Germany.

front from each event to the stations can be approximated as planar; and (c) P and S ray paths are coincident. Under these assumptions, given the differential arrival times between pairs of events detected at a network of sensors, an estimate of the local γ can be inferred by the following equation:

$$\delta t_S^i - \overline{\delta t_S} = \gamma(\delta t_P^i - \overline{\delta t_P}), \quad (1)$$

in which δt_P^i (or δt_S^i) is the difference between the arrival times of the P phases (or S phases) of a pair of events recorded at the ith station, whereas $\overline{\delta t_P}$ (or $\overline{\delta t_S}$) is the mean value of the differential P (or S) arrival times of the pair, averaged over all the stations. Following Lin and Shearer (2007), we define the demeaned differential arrival times as

$$\hat{\delta} t_{P,S}^i = \delta t_{P,S}^i - \overline{\delta t_{P,S}}. \quad (2)$$

Thus, equation (1) becomes

$$\hat{\delta} t_S^i = \gamma \hat{\delta} t_P^i. \quad (3)$$

Therefore, in ideal conditions, from the demeaned arrival times of all the pairs of events composing the cluster, the local γ can be inferred. Specifically, the points in the $\hat{\delta} t_P^i$ versus $\hat{\delta} t_S^i$ plane lie on a line through the origin, whose slope is γ. In real cases, noise and errors on the phase readings lead to scattered points in the $\hat{\delta} t_P$ versus $\hat{\delta} t_S$ plane, and γ must be inferred through a fitting procedure.

The relation between the differential travel times and arrival times at the ith station for a pair of events is

$$\delta t_{P,S}^i = \delta T_{P,S}^i + \delta T_0, \quad (4)$$

in which $\delta T_{P,S}^i$ is the difference in travel times and δT_0 is the difference in origin times between the two events of a pair. When $\delta T_0 \neq 0$, the differential arrival times for a pair of events lie on a line that does not cross the origin, as at the ith station:

$$\delta t_S^i = \gamma \delta t_P^i + \delta T_0(1-\gamma). \quad (5)$$

Subtracting the mean P and S differential arrival times from equation (5), δT_0 disappears because the relation between P and S mean differential arrival times is

$$\overline{\delta t_S} = \gamma \overline{\delta t_P} + \delta T_0(1-\gamma). \quad (6)$$

We remark that, whereas in the synthetic cases δT_0 is controlled *a priori* and thus the travel times are straightforwardly linked to the arrival times, in reality the origin times are mostly unknown or scarcely constrained and therefore the demeaning is essential.

Lin and Shearer (2007) tested the technique with a synthetic example consisting of a cluster of 27 earthquakes located at a depth of 10 km and contained within a cube of 0.2 km × 0.2 km × 0.2 km and 20 sensors randomly distributed on the free surface and located at epicentral distances ≤32 km from the cluster. The (differential) travel times were obtained adopting a 1D velocity model with both P and S velocity linearly increasing with depth but with different gradients, leading to a γ smoothly decreasing with depth (roughly from 1.8 to 1.6 in the 0–20 km depth range; see fig. 7 in Lin and Shearer, 2007). The results show that the slope in the δt_P versus δt_S plane for one pair of events is different from the expected γ because the P and S takeoff angles are not the same, violating one of the assumptions of the method. Nevertheless, the authors argued that such a bias tends to average out when the directions of the vectors connecting pairs of hypocenters within the earthquake cluster (intrahypocenter directions) are randomly distributed, resulting in a properly recovered γ value in their test when taking into account all possible event pairs. The method was then applied to the P and S arrival times of a real cluster of Californian earthquakes mostly located at depths of 5–10 km.

Synthetic Testing

Here we carry out further tests of the Lin and Shearer technique, applying it to an extended set of simulated differential P and S travel times. In detail, we adopt three 1D velocity models: (1) a homogeneous half-space model (HM), (2) a model similar to that proposed by Lin and Shearer (2007) defined in the 0–20 km range by a linearly decreasing γ and by a homogeneous model at larger depths (linear model [LM]), and (3) a model with three γ discontinuities (DM). Three subcases of DM are considered, distinguished by the magnitude of the γ discontinuities: 0.1 for DM1, 0.05 for DM2, and 0.02 for DM3. P- and S-wave velocity and corresponding γ of all models are shown in Figure 1a–d. In addition, we adopt a 3D velocity model simulating a simplified subduction zone, in which γ is 1.7 above the plate interface and 2 below it (subduction model [SM]; see Fig. 1e–g).

For each model, we fixed the position of a cluster of 55 events, whose hypocenters are randomly distributed in a cube. For HM, we center the cluster at a depth of 10 km with a spatial extent of 1 km × 1 km × 1 km. For LM, the cluster is centered at depths of 7.75, 9.75, 11.75, 15, and 25 km, with events contained in a cube of 0.5 km × 0.5 km × 0.5 km. In DM, the cluster is centered at depths of 25, 40, and 100 km and has a spatial extent of 1 km × 1 km × 1 km. In SM, the cluster is composed of 55 events representing selected aftershocks of the Tocopilla earthquake (14 November 2007, M_w 7.7, North Chile; Fuenzalida *et al.*, 2013). The hypocenters are centered at a depth of about 48 km within the oceanic plate and form a spatial cluster with an extent of ~3 km in all directions, with earthquake locations exactly as in the real aftershock sequence (see Figs. 1e–h and 2). All settings and corresponding results are summarized in Table 1. We fix the origin times of all events of the cluster at $t = 0$, thus $\delta T_0 = 0$ by design, and the differential travel times will coincide with the differential arrival times.

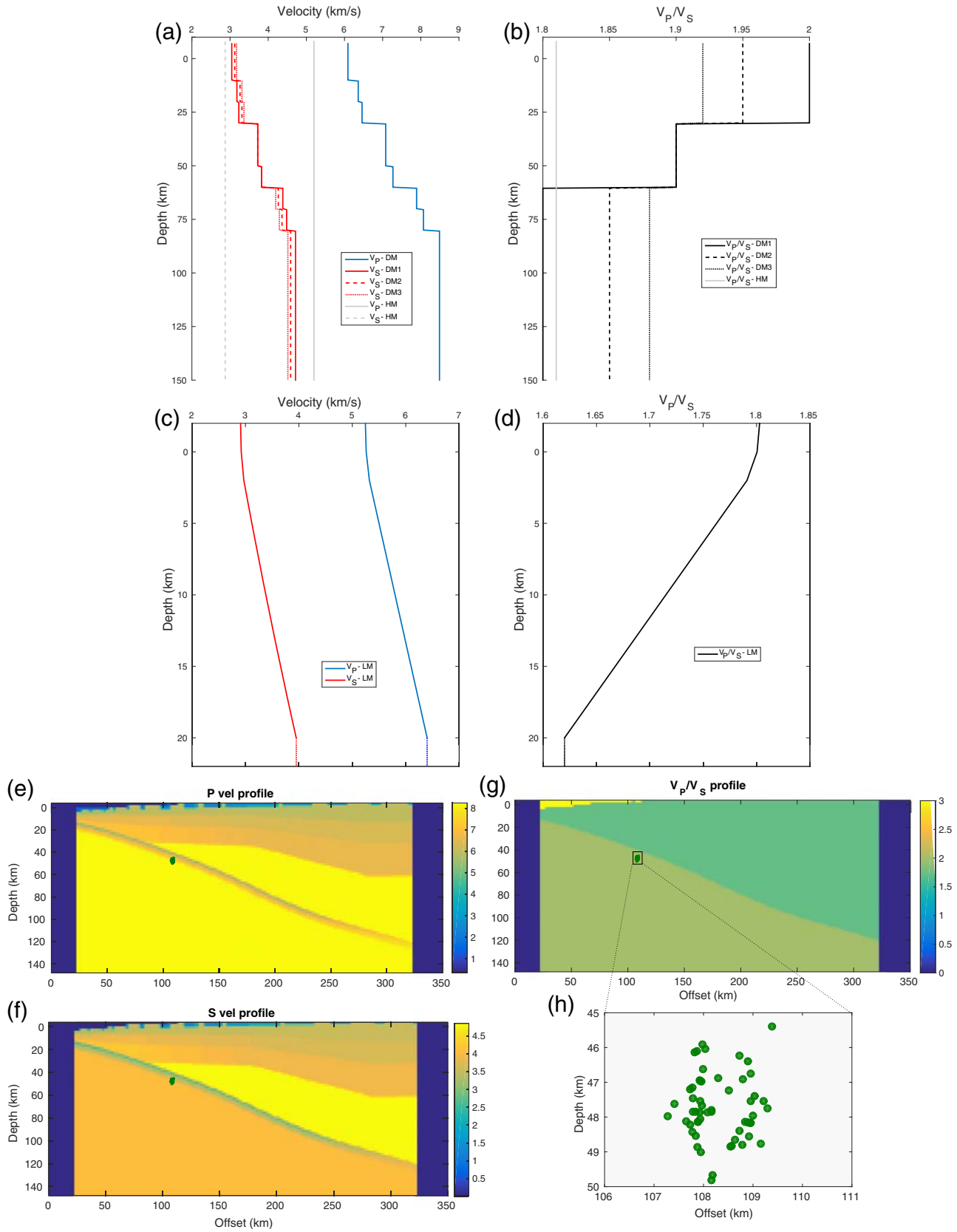

Figure 1. (a,b) *P* and *S* velocity and γ as function of depth for the 1D velocity models half-space model (HM) and discontinuity model (DM). (c,d) Same as (a,b) but for linear model (LM). For depths larger than 20 km, V_P, V_S, and γ uniformly assume the values at 20 km. (e–h) Sections of (e,f) *P* and *S* velocity and (g) γ for subduction model (SM) along a profile of constant latitude (23° S) (see Fig. 2). The circles show cluster of events (h). Zero on the *x* scale is fixed at 72° W. The color version of this figure is available only in the electronic edition.

Table 1
Results of Synthetic Tests Analyzed with Demeaning ($\hat{\delta}t_P, \hat{\delta}t_S$) and without Demeaning ($\delta t_P, \delta t_S$)

Scenario	Velocity Model	Depth Cluster (km)	Expected γ	γ with Demeaning	γ without Demeaning
HM-10	HM	10	1.81	1.81	1.81
LM-8	LM	7.75	1.735	**1.671**	1.717
LM-10	LM	9.75	1.715	**1.674**	1.731
LM-12	LM	11.75	1.696	**1.660**	1.699
LM-15	LM	15	1.667	1.651	1.676
LM-25	LM	25	1.620	1.635	1.625
DM1-25	DM1	25	2.0	2.011	1.995
DM1-40	DM1	40	1.90	**1.933**	1.899
DM1-100	DM1	100	1.80	**1.861**	1.807
DM2-25	DM2	25	1.95	1.960	1.952
DM2-40	DM2	40	1.90	1.919	1.905
DM2-100	DM2	100	1.85	**1.882**	1.854
DM3-25	DM3	25	1.92	1.924	1.921
DM3-40	DM3	40	1.90	1.908	1.901
DM3-100	DM3	100	1.88	1.893	1.880
SM-48	SM	48	2.0	**1.734**	**2.051**

Bold values mark the γ estimates with discrepancies, with the expected value larger than 0.03. HM, half-space model; LM, linear model; DM, discontinuity model.

The theoretical travel times are computed using a set of 32 stations from the permanent Integrated Plate Boundary Observatory (IPOC) network (International Federation of Digital Seismograph Networks [FDSN] network code: CX) and a temporary network (Task Force network–FDSN code: Y9) deployed in 2007 (see Fig. 2). We thus used a real station setting in order to establish the applicability of the technique in realistic conditions. The position of the event clusters for the scenarios HM, LM, and DM on the map is fixed as the barycenter of the station network.

Travel times from each station are computed on a 2 km × 2 km × 2 km grid using the finite-difference eikonal equation solver introduced by Vidale (1988), as implemented in the NonLinLoc package (Lomax *et al.*, 2000). The grid is large enough to contain all station and event locations. Final travel times are then determined by linear interpolation to the event location and rounded with a precision of 0.001 s.

Following Lin and Shearer (2007), we compute the best fit in the $\hat{\delta}t_P$ versus $\hat{\delta}t_S$ and δt_P versus δt_S planes by an iterative procedure. At the first iteration, the slope of the best fit is fixed to 3. At each iteration, in order to make the errors equal along the x and y axes, the y axis is divided by the slope of the best linear regression. The best fit is obtained by a least-squares (L2) approach, minimizing the sum of the squared orthogonal distances without fixing the intercept. Because our simulations do not include any artificial noise on the travel times, we assign the same weights to all points of the $\hat{\delta}t_P$ versus $\hat{\delta}t_S$ and δt_P versus δt_S planes; this is different from Lin and Shearer (2007), who weighted the outliers with an L1 metric. For the same reason, we calculate the arithmetic mean of the differential travel times at all stations to calculate $\overline{\delta t_{P,S}}$. The fitting procedure is repeated until convergence of the best fit, and the final value is assumed as an estimate of γ.

To ensure the stability of the procedure, we tried different values of the initial slope of the best-fitting line in the 1–5 range. In all cases, the numerical procedure converged to the same γ. Similarly, we verified that the results do not depend critically on the metric used for fitting. Indeed, using an L1 metric leads to the same γ as the value obtained with the L2 norm in most cases, or the difference in γ between the two metrics is well below the difference between the estimated and the real γ.

Results

In Figure 3a,c we show two examples (scenarios LM-10 and DM1-40; see Table 1) of the fitting procedure in the reduced δt_P versus δt_S plane. In Figure 3b,d, we plot the points in the reduced $\hat{\delta}t_P$ versus $\hat{\delta}t_S$ plane for the same scenarios, together with the best-fitting line. From the figure, it is clear that the slopes of the points before and after removing the mean values are different and that the value obtained before the demeaning is closer to the expected value than the slope in the $\hat{\delta}t_P$ versus $\hat{\delta}t_S$ plane. This behavior occurs in all cases investigated (see Table 1).

Comparing Figure 3a,c and 3b,d, it can be observed that the demeaning procedure shifts the points of the δt_P versus δt_S plane in a way that, on the $\hat{\delta}t_P$ versus $\hat{\delta}t_S$ plane, they occupy a segment with reduced width. The reason is that the demeaning tends to overlap all the points from each pair of events, which actually lay on lines whose slopes mismatch the real γ. This can be seen in Figure 4c,d, where we have plotted the distribution of the slopes of the lines fitting the points of each pair of events of the scenarios LM-10 and DM1-40 in the δt_P versus δt_S plane. The slopes mostly mismatch the expected γ. Therefore, as the final slope roughly

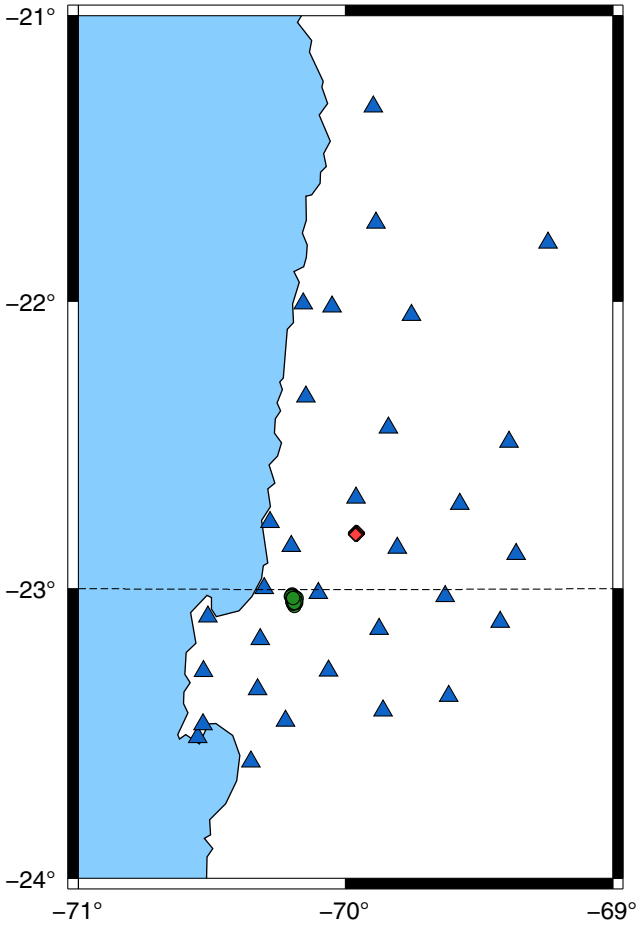

Figure 2. Assumed station distribution (triangles) and locations of event clusters. The diamonds mark the positions of the earthquake clusters for DM, LM, and HM scenarios, whereas the circles show the epicenters adopted for SM. The dotted horizontal line marks the profile adopted to obtain the sections of Figure 1e–h. The color version of this figure is available only in the electronic edition.

matches that of the points from the differential travel times of the individual pairs, it is not surprising that the final estimate of γ will not match the expected γ.

As mentioned by Lin and Shearer (2007), such a bias in the γ estimates comes from the different takeoff angles of P and S waves, which in turn leads to different paths of the two seismic phases, breaking one of the conditions on which the technique is based. This appears any time a γ gradient is introduced in the velocity model and is the reason why the only case in which the correct γ can be recovered also in the $\hat{\delta}t_P$ versus $\hat{\delta}t_S$ plane is the trivial case of a velocity model with homogeneous γ (see scenario HM-10 in Table 1).

Lin and Shearer (2007) argued that, as long as the intra-hypocenter directions are randomly distributed, the difference of the P and S takeoff angles, and thus also the consequently biased differential travel times, averages out. However, this averaging effect is only effective for the points in the δt_P versus δt_S plane and not for those in the $\hat{\delta}t_P$ versus $\hat{\delta}t_S$ plane. Indeed, in the original paper by Lin and Shearer (2007), the authors appear to have processed the nondemeaned differential travel times from the synthetic simulations, rather than the demeaned ones, with a nonhomogeneous velocity model. The effect of the mean removal is further demonstrated in Figure 4. The distributions of the $\delta t_P/\delta t_S$ ratios for scenarios LM-10 and DM1-40 are wide but broadly centered on the expected γ values of 1.715 and 1.90, respectively (Fig. 4a,b), explaining why the slopes of the best-fitting line in the δt_P versus δt_S plane are close to the expected values. On the other hand, the corresponding distributions in the $\hat{\delta}t_P$ versus $\hat{\delta}t_S$ plane (Fig. 4c,d) show that the slope of the differential arrival times for the individual pairs is mostly lower than 1.715 for LM-10 and larger than 1.90 for DM1-40. In other words, on average the differential P and S arrival times are in the expected ratio, but, in the $\hat{\delta}t_P$ versus $\hat{\delta}t_S$ plane, they are distributed in a way that the mean ratio for each event pair is mostly lower or larger than expected.

The source of this bias can be understood by considering a simplified example consisting of a layered medium in which both V_P and V_S are increasing with depth but V_P/V_S is decreasing (in the following, we distinguish the true velocity ratio V_P/V_S from its estimate γ). Without loss of generality, we define a coordinate system in which the first event of a pair is at the origin and the second is in the x–z plane (Fig. 5). Vector $\mathbf{e}$ with length a (interevent distance) and subtending angle α with the z axis points from the first to the second event. The directions of emitted P and S rays, $\hat{\mathbf{a}}_P$ and $\hat{\mathbf{a}}_S$, are described by azimuths $\phi_{P,S}$ and takeoff angles $\theta_{P,S}$. Because we assume a layered medium, both azimuths are the same, $\phi = \phi_P = \phi_S$. Further we define $\theta = \theta_P$ and takeoff angle difference $\delta = \theta_P - \theta_S$. In order for V_P/V_S to be decreasing with depth, the S gradient with depth must be larger than the P gradient. Thus S ray paths will be more strongly curved, and the takeoff vector of S rays will be steeper than that of P waves for the same distance, that is δ will be positive for the assumed negative gradient in V_P/V_S.

In Cartesian coordinates, we have

$$\hat{\mathbf{a}}_P = (\sin\theta\cos\phi,\ \sin\theta\sin\phi,\ -\cos\theta), \tag{7}$$

$$\hat{\mathbf{a}}_S = [\sin(\theta-\delta)\cos\phi,\ \sin(\theta-\delta)\sin\phi, -\cos(\theta-\delta)], \tag{8}$$

and

$$\mathbf{e} = a(\sin\alpha, 0, \cos\alpha). \tag{9}$$

The differential arrival time is simply the interevent distance projected along the P or S takeoff vector (that is, the dot product of $\mathbf{e}$ and $\hat{\mathbf{a}}_{P,S}$), scaled by the respective velocity:

$$\delta t_P = \frac{\mathbf{e}\cdot\hat{\mathbf{a}}_P}{V_P} = \frac{a}{V_P}(\sin\alpha\sin\theta\cos\phi - \cos\alpha\cos\theta) \tag{10}$$

and

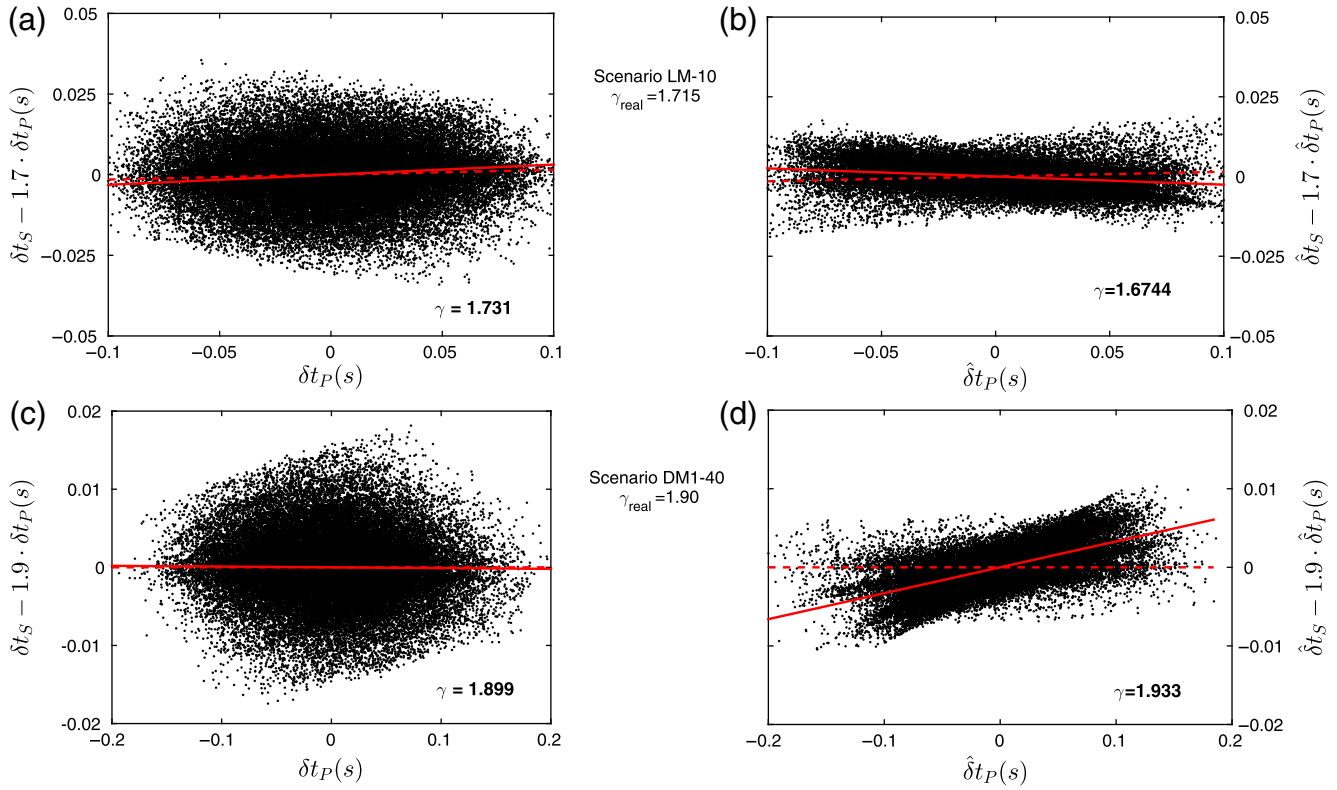

Figure 3. (a,b) Best-fitting line (continuous line) for the scenario LM-10 in the (a) δt_P versus $\delta t_S - 1.7\delta t_P$ and (b) $\hat{\delta} t_P$ versus $\hat{\delta} t_S - 1.7\hat{\delta} t_P$ planes. The slope corresponding to the real γ is plotted as a dashed line. (c,d) Same as (a,b) but for DM1-40 and in the (c) δt_P versus $\delta t_S - 1.9\delta t_P$ and (d) $\hat{\delta} t_P$ versus $\hat{\delta} t_S - 1.9\hat{\delta} t_P$ planes. The color version of this figure is available only in the electronic edition.

$$\delta t_S = \frac{\mathbf{e} \cdot \hat{\mathbf{a}}_S}{V_S} = \frac{a}{V_S}[\sin\alpha \sin(\theta - \delta)\cos\phi - \cos\alpha\cos(\theta - \delta)]. \tag{11}$$

Demeaning will remove the influence of differences in origin time according to equation (6) but can also affect the γ estimate. We consider the case of perfectly even azimuthal coverage for a given narrow range in the takeoff angle θ. The mean value of P will then be given by

$$\overline{\delta t_P} = \frac{a}{V_P}(\sin\alpha \sin\theta < \cos\phi > - \cos\alpha\cos\theta), \tag{12}$$

in which the angle operator implies averaging over all stations. The first term disappears in the mean because $< \cos\phi >= 0$ for perfectly balanced azimuthal coverage, thus

$$\overline{\delta t_P} = -\frac{a}{V_P}\cos\alpha\cos\theta \tag{13}$$

and finally

$$\hat{\delta} t_P = \delta t_P - \overline{\delta t_P} = \frac{a}{V_P}\sin\alpha\sin\theta\cos\phi. \tag{14}$$

Equivalently,

$$\hat{\delta} t_S = \frac{a}{V_S}\sin\alpha\sin(\theta - \delta)\cos\phi. \tag{15}$$

By definition, the demeaned differential arrival times lie on a line through the origin; and, by equation (3), we can thus calculate γ from any station by

$$\gamma = \frac{\hat{\delta} t_S}{\hat{\delta} t_P} = \frac{V_P}{V_S}\left(\frac{\sin(\theta - \delta)}{\sin\theta}\right) = \frac{V_P}{V_S}\left(\frac{\sin\theta\cos\delta - \cos\theta\sin\delta}{\sin\theta}\right), \tag{16}$$

in which the second part of the identity makes use of standard trigonometric identities. If we additionally assume the gradient of V_P/V_S to be small, P and S will have similar takeoff angles and δ will consequently be small. By approximating, to first order in δ, $\sin\delta = \delta$, and $\cos\delta = 1$, we finally obtain a simple approximate expression:

$$\gamma = \frac{V_P}{V_S}\left(1 - \frac{\delta\cos\theta}{\sin\theta}\right). \tag{17}$$

For downgoing rays (takeoff angles $\theta < 90°$), the factor in the parentheses is less than 1 and γ underestimates the true V_P/V_S value. The reverse is true for upgoing rays; that is, for

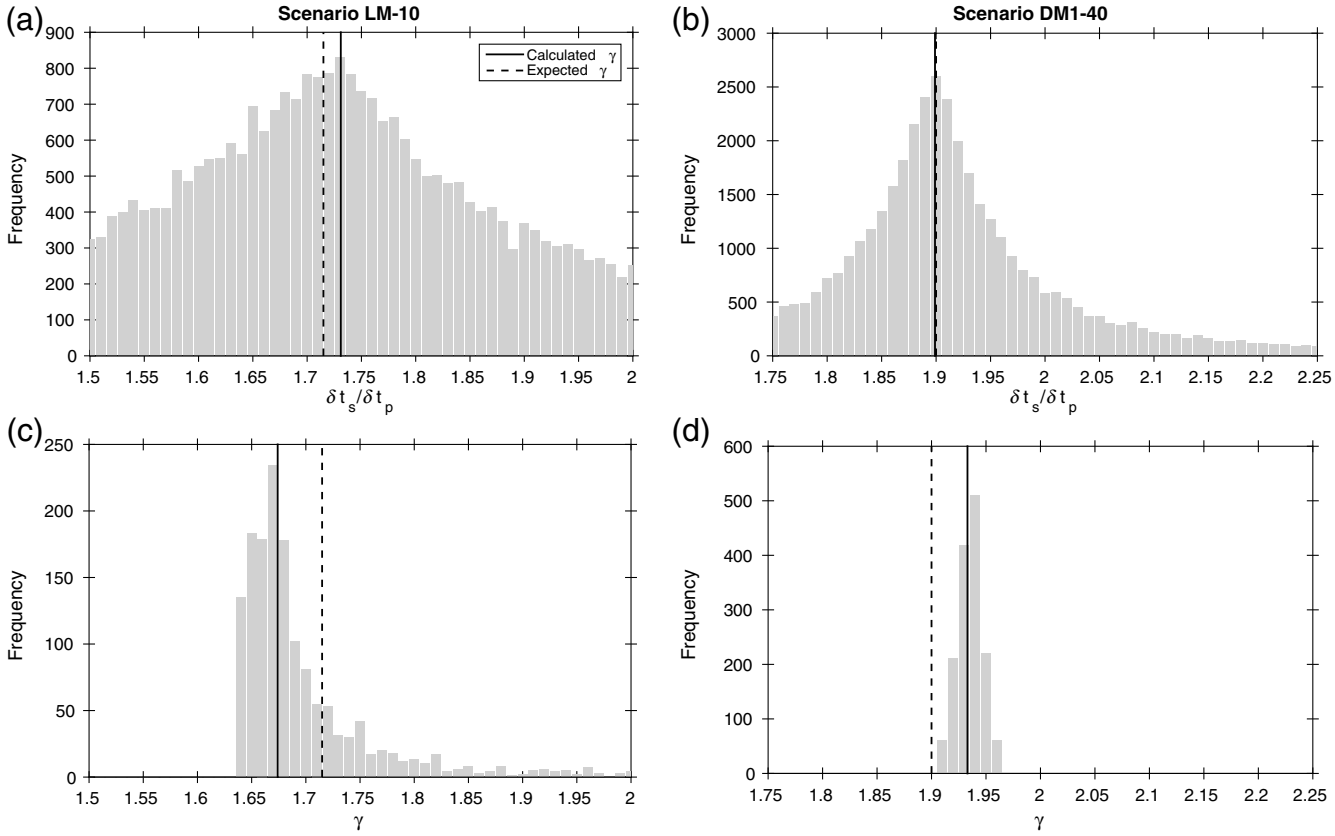

Figure 4. (a,b) Distribution of the $\delta t_P/\delta t_S$ ratios for all pairs in scenarios (a) LM-10 and (b) DM1-40; (c,d) distribution of the slope of the lines fitting the points in the δt_P versus δt_S plane of each individual pair of events for the scenarios (c) LM-10 and (d) DM1-40. The expected γ for the two scenarios are graphically indicated by the dashed vertical line, whereas the continuous line shows the calculated γ.

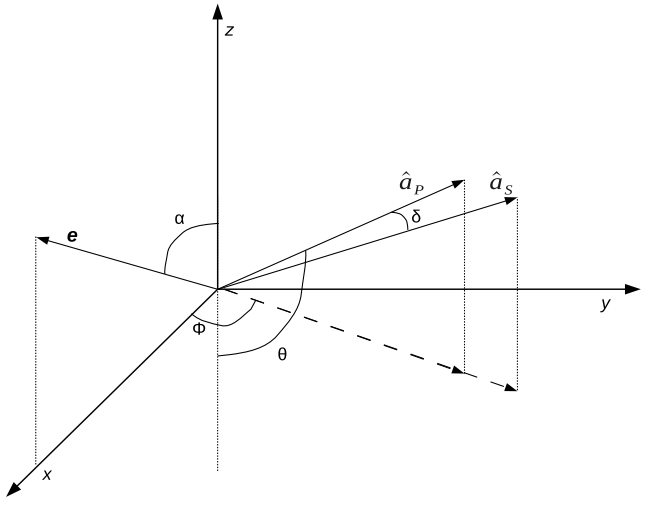

Figure 5. Sketch displaying the intrahypocenter vector (**e**) and the *P* and *S* takeoff vectors ($\hat{\mathbf{a}}_{P,S}$). The interevent vector **e** is in the *x*-*z* plane and forms an angle of α with the *z* axis. $\hat{\mathbf{a}}_P$ and $\hat{\mathbf{a}}_S$ have takeoff angles of $\theta_P = \theta$ and $\theta_S = \theta - \delta$, respectively, and the same azimuth ϕ.

these observations, γ will overestimate the true V_P/V_S. If the V_P/V_S ratio is increasing with depth, then $\delta < 0°$ and the opposite biases result. Notably, expressions (16) and (17) do not depend on the interevent directions, meaning this bias cannot be reduced by having a good distribution of interhypocenter directions.

Returning to the synthetic scenarios, *P* and *S* takeoff angles are both $<90°$ for scenario LM-10 and the resultant γ is underestimated, whereas the takeoff angles are mostly $>90°$ for DM1-40 and γ results overestimated. The bias on γ as function of the takeoff angles is investigated further in Figure 6, which shows *P* and *S* mean takeoff angles for all stations for scenarios LM-8, LM-15, and LM-25. For LM-8 and LM-15, the takeoff angles are mostly between 50° and 90° and γ is underestimated, whereas in scenario LM-25 the takeoff angles are mostly between 90° and 130° and γ is overestimated. The bias due to the effects of the different *P* and *S* takeoff angles would be reduced if (1) the takeoff angles are concentrated around 90°; (2) there is a good balance of takeoff angles below and above 90°, resulting in partial cancellation of the biasing effects on γ; or (3) the difference between *P* and *S* takeoff angles is $\simeq 0$. However, in nearly all realistic settings, in which seismic stations generally are confined to the surface or near surface, such a balance of up- and downgoing rays is almost impossible to achieve.

Although both demeaned and nondemeaned data will result in biased results, the averaging out of the biasing effects due to paths experiencing opposite effects works much better for nondemeaned data, as can be appreciated by com-

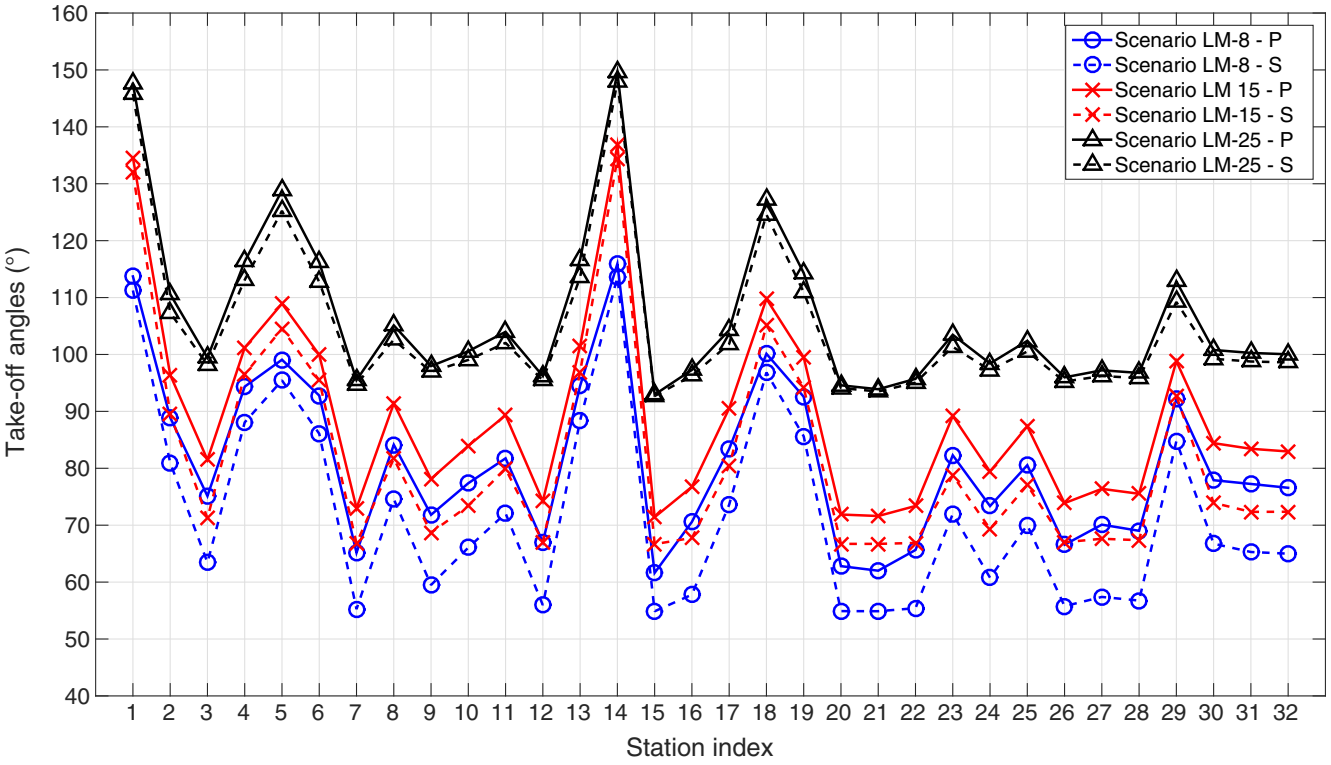

Figure 6. Mean takeoff angles (averaged over the 55 events of the cluster) of the *P* and *S* ray paths connecting the cluster with all stations in the LM velocity model. The results for scenarios LM-8, LM-15, and LM-25 are plotted. 0° means a ray emitted downward, 180° means a ray emitted upward. As expected, *P* takeoff angles are always larger than *S* takeoff angles, and the discrepancy decreases as the cluster becomes deeper. The color version of this figure is available only in the electronic edition.

paring the demeaned and nondemeaned results presented in Table 1. This difference is especially pronounced in the more realistic scenario SM-48, in which the estimated γ value was off by nearly 0.27, too large to allow any meaningful interpretation of the result, even though for this test a complete and noise-free dataset was assumed. Unfortunately, as pointed out above, the estimate of γ from the fitting of the points in the δt_P versus δt_S plane can be done only in the cases in which the exact origin times of the events are known (as in our simulations, in which all earthquakes occur simultaneously at $t = 0$); however, in real cases, the origin times are unknown or known with large errors, such that demeaning cannot be avoided. Because the number of earthquake pairs (and thus mean values) is much larger than the number of unknown origin times, one might expect that explicitly solving for origin time corrections rather than demeaning would result in a situation closer to the nondemeaned case. However, we tested this approach for some scenarios and found that it did not result in improved estimates of γ.

We remark also that real cases normally show more complex conditions than those included in the simulations performed here. For example, we processed all possible differential travel times (rays from each event to each station). This is normally not the case, because the arrival times at the furthest stations are often unclear (if even visible). Moreover, the hypocenters often occur in linear or planar spatial distributions, following the geometries of the seismogenic structures, thus not fulfilling the condition of well-distributed interevent directions. In addition, we excluded the presence of noise in our tests.

Conclusions

Both theoretical considerations and synthetic tests in simple models with benign geometries (layered models and cubic event clusters) indicate that the technique proposed by Lin and Shearer (2007) returns biased estimates, even where interevent direction vectors are well distributed. This bias originates from the difference between *P* and *S* takeoff angles, which is an inevitable consequence of depth-dependent V_P/V_S ratios. When demeaning is applied, the slope in the $\hat{\delta}t_P$ versus $\hat{\delta}t_S$ plane is independent of the interevent directions such that the event distribution does not contribute to effective averaging. Instead, in order to avoid bias, takeoff angles would have to be well distributed between 0° and 180° (down- and upgoing rays) or all be near horizontal, a situation rarely found in typical seismological datasets. In the synthetic tests, differences between true and estimated γ values were up to 0.06 for simple geometries and 0.27 for a more realistic case including an elongated cluster and a dipping layer in the velocity model. In reality, the fidelity of the γ estimates is likely to be further degraded by missing ob-

servations, uneven azimuthal coverage, and measurement uncertainty.

Given a 3D distributed cluster of earthquakes and a set of stations surrounding the cluster, better estimates of γ could theoretically be obtained if the differential travel times $\delta T_{P,S}$ could be computed, which implies that the origin times of the events must be fixed by independent constraints. In this case, the demeaning can be avoided and the effects of the different P and S takeoff angles average out more effectively. Although the method of Lin and Shearer (2007) might work in narrow circumstances (e.g., where borehole measurements provide the required wide sampling of takeoff angles), results derived with this method have to be treated with caution, and we recommend avoiding it for typical local seismic network geometries.

Data and Resources

Data processing was mostly performed by MATLAB (www.mathworks.com/products/matlab, last accessed April 2016). Figure 2 has been made using Generic Mapping Tools v.4.5.13 (http://www.soest.hawaii.edu/gmt/, last accessed April 2016; Wessel and Smith, 1998). Travel times of synthetic tests were computed using the NonLinLoc package (Lomax *et al.*, 2000). Earthquake hypocenters of Figure 1e–h were obtained by relocating (by a double-difference technique) a subset of aftershocks of the Tocopilla event (Fuenzalida *et al.*, 2013).

Acknowledgments

Funding for this work was provided by the German Research Foundation (DFG) for the MARISCOS bundle project, TI 316/1-1.

References

Audet, P., M. G. Bostock, N. I. Christensen, and S. M. Peacock (2009). Seismic evidence for overpressured subducted oceanic crust and megathrust fault sealing, *Nature* **457,** no. 7225, 76–78.

Christensen, N. I. (1996). Poisson's ratio and crustal seismology, *J. Geophys. Res.* **101,** no. B2, 3139–3156.

Dahm, T., and T. Fischer (2014). Velocity ratio variations in the source region of earthquake swarms in NW Bohemia obtained from arrival time double-differences, *Geophys. J. Int.* **196,** no. 2, 957–970.

Eberhart-Phillips, D., D. Han, and M. D. Zoback (1989). Empirical relationships among seismic velocity, effective pressure, porosity, and clay content in sandstone, *Geophysics* **54,** no. 1, 82–89.

Fuenzalida, A., B. Schurr, M. Lancieri, M. Sobiesiak, and R. Madariaga (2013). High-resolution relocation and mechanism of aftershocks of the 2007 Tocopilla (Chile) earthquake, *Geophys. J. Int.* **194,** no. 2, 1216–1228.

Hacker, B. R., G. A. Abers, and S. M. Peacock (2003). Subduction factory 1. Theoretical mineralogy, densities, seismic wave speeds, and H_2O contents, *J. Geophys. Res.* **108,** no. B1, doi: 10.1029/2001JB001127.

Hickman, S., and W. Ellsworth (2010). Scientific drilling into the San Andreas fault zone, *Eos Trans. AGU* **91,** no. 22, 197–199.

Lachenbruch, A. H. (1980). Frictional heating, fluid pressure, and the resistance to fault motion, *J. Geophys. Res.* **85,** no. B11, 6097–6112.

Lay, T., and H. Kanamori (1981). An asperity model of large earthquake sequences, in *Earthquake Prediction–An International Review*, D. Simpson and P. Richards (Editors), Vol. 4, Maurice Ewing Series, American Geophysical Union, Washington, D.C., 579–592.

Lin, G., and P. M. Shearer (2007). Estimating local V_P/V_S ratios within similar earthquake clusters, *Bull. Seismol. Soc. Am.* **97,** no. 2, 379–388.

Lin, G., and P. M. Shearer (2009). Evidence for water-filled cracks in earthquake source regions, *Geophys. Res. Lett.* **36,** no. 17, doi: 10.1029/2009GL039098.

Lomax, A., A. J. Virieux, P. Volant, and C. Berge (2000). Probabilistic earthquake location in 3D and layered models: Introduction of a Metropolis-Gibbs method and comparison with linear locations, in *Advances in Seismic Event Location*, C. H. Thurber and N. Rabinowitz (Editors), Kluwer, Amsterdam, The Netherlands, 101–134.

O'Connell, R. J., and B. Budiansky (1974). Seismic velocities in dry and saturated cracked solids, *J. Geophys. Res.* **79,** no. 35, 5412–5426.

Peacock, S. M., N. I. Christensen, M. G. Bostock, and P. Audet (2011). High pore pressures and porosity at 35 km depth in the Cascadia subduction zone, *Geology* **39,** no. 5, 471–474.

Scholz, C. H. (1988). Earthquakes and friction laws, *Nature* **391,** no. 6662, 37–42.

Schwartz, S. Y., and J. M. Rokosky (2007). Slow slip events and seismic tremor at circum-Pacific subduction zones, *Rev. Geophys.* **45,** no. 3, doi: 10.1029/2006RG000208.

Shearer, P. M. (1988). Cracked media, Poisson's ratio and the structure of the upper oceanic crust, *Geophys. J. Int.* **92,** no. 2, 357–362.

Vidale, J. (1988). Finite-difference calculation of travel times, *Bull. Seismol. Soc. Am.* **78,** 2062–2076.

Wang, X. Q., A. Schubnel, J. Fortin, E. C. David, Y. Gueguen, and H. K. Ge (2012). High V_P/V_S ratio: Saturated cracks or anisotropy effects? *Geophys. Res. Lett.* **39,** no. 11, doi: 10.1029/2012GL051742.

Wessel, P., and W. H. F. Smith (1998). New, improved version of Generic Mapping Tools released, *Eos Trans. AGU* **79,** no. 47, 579.

Helmholtz-Zentrum Potsdam
Deutsches GeoForschungsZentrum GFZ
Section 2.4, Seismology
Telegrafenberg, A3 101
D-14473 Potsdam, Germany
mpalo@gfz-potsdam.de
tilmann@gfz-potsdam.de
(M.P., F.T.)

Helmholtz-Zentrum Potsdam
Deutsches GeoForschungsZentrum GFZ
Section 3.1, Lithosphere Dynamics
Telegrafenberg, C 221
D-14473 Potsdam, Germany
bernd.schurr@gfz-potsdam.de
(B.S.)

Manuscript received 2 November 2015;
Published Online 10 May 2016